SIAM J. APPL. MATH.
Vol. 68, No. 1, pp. 292–310

CONVECTIVE STABILIZATION OF A LAPLACIAN MOVING BOUNDARY PROBLEM WITH KINETIC UNDERCOOLING*

UTE EBERT†, BERNARD MEULENBROEK‡, AND LOTHAR SCHÄFER§

Abstract. We study the shape stability of disks moving in an external Laplacian field in two dimensions. The problem is motivated by the motion of ionization fronts in streamer-type electric breakdown. It is mathematically equivalent to the motion of a small bubble in a Hele–Shaw cell with a regularization of kinetic undercooling type, namely, a mixed Dirichlet–Neumann boundary condition for the Laplacian field on the moving boundary. Using conformal mapping techniques, linear stability analysis of the uniformly translating disk is recast into a single PDE which is exactly solvable for certain values of the regularization parameter. We concentrate on the physically most interesting exactly solvable and nontrivial case. We show that the circular solutions are linearly stable against smooth initial perturbations. In the transformation of the PDE to its normal hyperbolic form, a semigroup of automorphisms of the unit disk plays a central role. It mediates the convection of perturbations to the back of the circle where they decay. Exponential convergence to the unperturbed circle occurs along a unique slow manifold as time $t \to \infty$. Smooth temporal eigenfunctions cannot be constructed, but excluding the far back part of the circle, a discrete set of eigenfunctions does span the function space of perturbations. We believe that the observed behavior of a convectively stabilized circle for a certain value of the regularization parameter is generic for other shapes and parameter values. Our analytical results are illustrated by figures of some typical solutions.

Key words. moving boundaries, kinetic undercooling, Laplacian growth, streamer discharges, convective stabilization

AMS subject classifications. 37L15, 37L25, 76D27, 80A22, 78A20

DOI. 10.1137/070683908

1. Introduction.

1.1. Problem formulation in physical and mathematical context. The mathematical model considered in this paper is motivated by the physics of electric breakdown of simple gases like nitrogen or argon [1, 2, 3, 4, 5]. During the initial "streamer" phase of spark formation, a weakly ionized region extends in a strong externally applied electric field. As the ionized cloud is electrically conducting, it screens the electric field from its interior by forming a thin surface charge layer. This charged layer moves by electron drift within the local electric field and creates additional ionization, i.e., additional electron-ion pairs, by collisions of fast electrons with neutral molecules. We here approximate the ionized and hence conducting bulk of the streamer as equipotential. In the nonionized and hence electrically neutral region outside the streamer, the electric field obeys the Laplace equation. The thin surface charge layer can be approximated as an interface which moves according to

*Received by the editors June 19, 2006; accepted for publication (in revised form) July 16, 2007; published electronically November 7, 2007. Both the exact solution (4.4) and the slow manifold (4.15) were briefly presented in *Physical Review Letters* [14].
http://www.siam.org/journals/siap/68-1/68390.html

†CWI, MAS, P.O. Box 94079, 1090 GB Amsterdam, The Netherlands, and Department of Applied Physics, Technical University Eindhoven, 5600 MB Eindhoven, The Netherlands (ebert@cwi.nl).

‡CWI, MAS, P.O. Box 94079, 1090 GB Amsterdam, The Netherlands. Current address: Department of Applied Mathematics, Delft University of Technology, 2600 AA Delft, The Netherlands (B.J.Meulenbroek@tudelft.nl). This author's research was supported by a Ph.D. position from CWI Amsterdam.

§Department of Theoretical Physics, Universität Duisburg–Essen, Lotharstr. 1, 47048 Duisburg, Germany (lsphy@theo-phys.uni-essen.de).

the electric field extrapolated from the neutral region onto the interface. We therefore are concerned with a typical moving boundary problem.

Such moving boundary problems occur in various branches of physics, chemistry, or biology. The most extensively studied examples are viscous fingering observed in two-fluid flows [6] or the Stefan problem of solidification from an undercooled melt [7]. Other physical phenomena like the motion of voids in current carrying metal films [8] lead to similar mathematical models [9].

We here discuss the streamer model in two spatial dimensions, where in the simplest "unregularized" version the basic equations coincide with those describing the motion of a small bubble in a liquid streaming through a Hele–Shaw cell [10, 11, 12, 13], which is a special case of two-fluid flow. The unregularized streamer model has been discussed in [4, 14]. Restriction to two dimensions in space allows us to use standard conformal mapping techniques [6, 15] to reduce the moving boundary problem to the analysis of the time dependence of the conformal map that maps the unit disk to the exterior of the streamer.

It is well known that unregularized moving boundary problems of this type are mathematically ill posed [15], in the sense that the moving interface generically develops cusps within finite time which leads to a breakdown of the model. To suppress such unphysical behavior, the models are regularized by imposing nontrivial boundary conditions on the interface. For viscous fingering typically some curvature correction to the interfacial energy is considered. For the streamer problem a mixed Dirichlet–Neumann boundary condition can be derived [14, 16] by analyzing the variation of the electric potential across the screening layer. Such a boundary condition is well known from the Stefan problem, where it is termed "kinetic undercooling." It rarely has been considered for Hele–Shaw-type problems. There are strong hints [15, 17, 18, 19] but no clear proof that it suppresses cusp formation. In particular, it has been shown that an initially smooth interface stays smooth for some finite time interval.

Here we consider the linear stability of uniformly translating circles in a Laplacian potential φ that approaches a constant slope $\varphi \propto x$ far from the circle; this means that the electric field $\mathbf{E} = -\nabla\varphi$ is constant far from the circle. Though this field breaks radial symmetry, uniformly translating circles are exact solutions of the regularized problem [14]. However, perturbations of these circles do not simply grow or decay locally as on a planar front or on circles in a radially symmetric force field [17, 18], but are also convected along the boundary; this convection turns out to be a determining part of the dynamics. Though physical streamers are elongated objects frequently connected to an electrode, the front part of a streamer is well approximated by a circular shape. Since it is this part that determines the dynamics, our analysis should be relevant also for more realistic shapes like fingers where no closed analytical solutions of the regularized uniformly translating shape are known [19]. In what follows we will use the term "streamer" to denote the translating circles, being aware that this is a slight abuse of the term.

1.2. Overview of content and structure of the paper. Regularization of the streamer model introduces some parameter ϵ that measures the effective width of the interface relative to the typical size of the ionized region. The regularized problem allows for a class of solutions of the form of uniformly translating circles, and linear stability analysis of these solutions can be reduced to solving a single PDE. For the special case $\epsilon = 1$, the general solution of this PDE can be found analytically, as we briefly discussed in [14]. The present paper is restricted to this special case as well.

The main results of the letter [14] are the following: The dynamics of infinitesi-

mal perturbations is governed by a subgroup of the automorphisms of the unit disk. Generically, these automorphisms convect the perturbations to the back of the moving body. Initially, perturbations might grow, but they decay exponentially for $t \to \infty$. Furthermore, this final convergence back to the unperturbed circle follows some universal slow manifold.

The present paper contains a detailed derivation, discussion, and extension of the results presented in [14]. Furthermore, the analyticity and completeness of temporal eigenfunctions and the Fourier decomposition of perturbations are discussed, limit cases of the dynamics are worked out analytically, and results are demonstrated in a set of figures.

In detail, the time evolution determined by a PDE is often analyzed in terms of temporal eigenfunctions. For the present problem in a space of functions representing smooth initial perturbations of the moving circle, no such eigenfunctions exist. They can be constructed only if we allow for singularities on the boundary. We find here that a subset of these functions with time dependence $e^{-n\tau}$, $n \in \mathbf{N}_0$, is intimately related to the asymptotic convergence of the perturbations. These functions show singularities only at the backside of the circle, and the front part of any smooth perturbation can be expanded in this set of functions. The spatial domain of convergence of this expansion increases with time and, asymptotically for $t \to \infty$, it covers almost the whole streamer. In this restricted sense these eigenfunctions form a complete set.

These results dealing with infinitesimal perturbations, of course, do not imply the asymptotic stability of the circular shape against finite perturbations. To solve this problem, the full nonlinear theory must be considered. Nevertheless, a first hint might be gained by considering the evolution of a finite perturbation under the linearized dynamics. Due to the conformal mapping involved, the absence of cusps under this evolution is not a completely trivial question. We show here that for a large range of smooth initial conditions, the shape of the streamer stays smooth under the linearized dynamics.

All the present work deals with the exactly solvable case $\epsilon = 1$, whereas the physically most interesting case is $\epsilon \ll 1$. We believe, however, that the features we could identify explicitly for $\epsilon = 1$ are generic for all $\epsilon > 0$. In particular, the subgroup of automorphisms of the unit circle leads to the basic mechanism of convective stabilization, it is for all $\epsilon > 0$ intimately related to the characteristic curves of the PDE, and it also governs the dynamics in another exactly solvable case, namely, for $\epsilon = \infty$. Furthermore, it can be shown [20] that the temporal eigenvalues $\lambda_n(\epsilon)$ emerging from $\lambda_n(1) = -n$ stay negative for all $\epsilon > 0$, which also indicates that the circle might be asymptotically stable for arbitrary $\epsilon > 0$.

This paper is organized as follows. In section 2 we introduce the model, and the linear stability analysis of translating circles is carried through in section 3. These two sections are extended versions of [14]. Analytical results based on the PDE of linear stability analysis are derived in section 4, in particular, center of mass motion, internal motion, (non)analyticity and completeness of eigenfunctions, intermediate growth and asymptotic decay of perturbations, Fourier representation, and motion of nonanalytical points in the complex plane of the conformal map. These dynamic features are illustrated by explicit examples in section 5. The appendix contains a discussion of the case $\epsilon = \infty$.

2. Physical model and conformal mapping approach.

2.1. The model. We assume the ionized bulk of the streamer to be a compact, simply connected domain $\bar{\mathcal{D}}_i$ of the (x, y)-plane (see Figure 2.1). Outside the streamer,

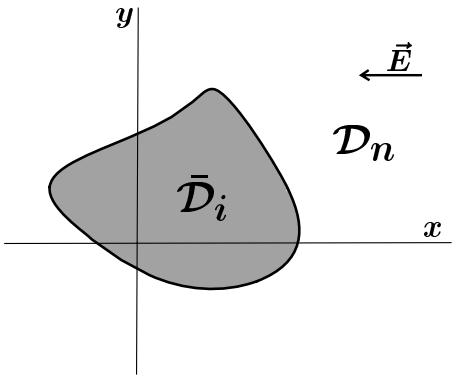

FIG. 2.1. *Geometry of the streamer model; $\vec{E}$ is the constant far field.*

i.e., in the open domain $\mathcal{D}_n$, there are no charges and the electric potential obeys the Laplace equation

$$\Delta\varphi = 0 \quad \text{for } (x,y) \in \mathcal{D}_n. \tag{2.1}$$

The streamer moves in an external electric field that becomes homogeneous far from the ionized body; therefore the electric potential φ at infinity obeys the boundary condition

$$\varphi \to E_0 x + \text{const} \quad \text{for } \sqrt{x^2+y^2} \to \infty. \tag{2.2}$$

This condition excludes a contribution to φ diverging as $\ln(x^2+y^2)$, which implies that the total charge due to the sum of all electrons and ions vanishes within $\bar{\mathcal{D}}_i$ and that the far field has the form

$$\vec{E} = -\nabla\varphi \to -E_0\hat{\mathbf{x}},$$

where $\hat{\mathbf{x}}$ is the unit vector in the x-direction. On the surface of the streamer we impose the boundary condition

$$\varphi = \ell\,\hat{\mathbf{n}}\cdot\nabla\varphi, \tag{2.3}$$

where $\hat{\mathbf{n}}$ is the unit vector normal to the surface pointing into $\mathcal{D}_n$. Here as well as in (2.4) below it is understood that the surface is approached from $\mathcal{D}_n$. As mentioned in the introduction, this boundary condition results from the analysis of the variation of the potential across the interface, and the length parameter ℓ can be interpreted as the effective thickness of the screening layer. The case $\ell = 0$ corresponds to the unregularized case with a pure Dirichlet condition on the moving boundary. Dynamics is introduced via the relation

$$v_n = \hat{n}\cdot\nabla\varphi, \tag{2.4}$$

which holds on the boundary and determines its normal velocity v_n. This defines our model. For further discussion of its physical background, we refer to [1, 2, 3, 4, 5, 16]. Now obviously, E_0 can be absorbed into a rescaling of the potential φ and of the time scale inherent in the velocity v_n; therefore we henceforth take $E_0 = 1$. Clearly the model defined here is most similar to a model of the motion of a small bubble in a Hele–Shaw cell [11, 12], except that the boundary condition (2.3) is of the form of a kinetic undercooling condition [17, 18].

2.2. Conformal mapping. A standard approach to such moving boundary problems proceeds by conformal mapping [6, 14]. We identify the (x, y)-plane with the closed complex plane $z = x+iy$, and we define a conformal map $f(\omega, t)$ that maps the unit disk $\mathcal{U}_\omega$ in the ω-plane to $\mathcal{D}_n$ in the z-plane, with $\omega = 0$ being mapped on $z = \infty$:

$$z = f(\omega, t) = \frac{a_{-1}(t)}{\omega} + \hat{f}(\omega, t), \quad a_{-1}(t) > 0. \tag{2.5}$$

Here the function $\hat{f}$ is holomorphic for $\omega \in \mathcal{U}_\omega$, and we assume that the derivatives ∂_ω^n of all orders n exist on the unit circle $\partial\mathcal{U}_\omega$. This restricts our analysis to smooth boundaries of the streamer. (Weaker assumptions on boundary behavior will be discussed briefly in section 4.8.) We recall that the closed physical boundary can now be retrieved as $x_\alpha(t) = \Re f(e^{i\alpha}, t)$ and $y_\alpha(t) = \Im f(e^{i\alpha}, t))$, where the interface parametrization with the real variable $\alpha \in [0, 2\pi[$ is fixed by the conformal map.

By virtue of (2.1), the potential φ restricted to $\mathcal{D}_n$ is a harmonic function; therefore it is the real part of some analytic function $\tilde{\Phi}(z, t)$, which under the conformal map (2.5) transforms into

$$\Phi(\omega, t) = \tilde{\Phi}\left(f(\omega, t)\right) = \frac{a_{-1}(t)}{\omega} + \hat{\Phi}(\omega, t). \tag{2.6}$$

Here the holomorphic function $\hat{\Phi}$ obeys the same conditions as $\hat{f}$ above. The pole results from the boundary condition (2.2) with $E_0 = 1$ and (2.5).

Conditions (2.3) and (2.4) take the form

$$|\omega\partial_\omega f|\, \Re[\Phi] = -\ell\, \Re\left[\omega\partial_\omega \Phi\right] \quad \text{for } \omega \in \partial\mathcal{U}_\omega, \tag{2.7}$$

$$\Re\left[\frac{\partial_t f}{\omega\partial_\omega f}\right] = \frac{\Re\left[\omega\partial_\omega\Phi\right]}{\left|\omega\partial_\omega f\right|^2} \quad \text{for } \omega \in \partial\mathcal{U}_\omega. \tag{2.8}$$

Equations (2.5)–(2.8) form the starting point of our analysis.

3. Linear stability analysis of translating circles.

3.1. Uniformly translating circles. A simple solution of (2.7), (2.8) takes the form

$$\begin{cases} f^{(0)}(\omega, t) = \dfrac{R}{\omega} + \dfrac{2R}{R+\ell}\, t, \\ \Phi^{(0)}(\omega, t) = R\left[\dfrac{1}{\omega} - \dfrac{R-\ell}{R+\ell}\,\omega\right]. \end{cases} \tag{3.1}$$

In physical coordinates x and y, it describes circles of radius $R > 0$ centered at $x(t) = v_0 t$ and moving with velocity $v_0 = 2R/(R+\ell)$ in direction $\hat{\mathbf{x}}$. Thus the point $\omega = 1$ maps to a point at the front, and the point $\omega = -1$ maps to a point at the back of the streamer. These points will play a crucial role in our analysis.

We note that the one-parameter family (3.1) of solutions parametrized by R, which is found in the regularized model, is a subset of the two-parameter family found in the unregularized case $\ell = 0$. As is well known, for $\ell = 0$ all ellipses with one axis parallel to $\hat{\mathbf{x}}$ are uniformly translating solutions [10].

3.2. Derivation of the operator $\boldsymbol{\mathcal{L}_\epsilon}$ for linear stability analysis. We now derive the equation governing the evolution of infinitesimal perturbations of the circles

(3.1). In general, the parameter R can become time dependent. We use the ansatz

$$\begin{cases} f(\omega,t) = \dfrac{R(t)}{\omega} + x(t) + \eta\,\beta(\omega,t)\,, \\ \Phi(\omega,t) = R(t)\left[\dfrac{1}{\omega} - \dfrac{R(t)-\ell}{R(t)+\ell}\,\omega + \eta\,\chi(\omega,t)\right], \\ \partial_t x(t) = \dfrac{2R(t)}{R(t)+\ell}, \quad R(t) > 0, \end{cases} \tag{3.2}$$

where β and χ are holomorphic functions of ω and where η is a small parameter. However, working to first order in η it is found that R stays constant. This results from the fact that the dynamics embodied in (2.8) strictly conserves the area $|\bar{\mathcal{D}}_i|$ of the streamer, which in this context is equivalent to the temporal conservation of the zero order Richardson moment [13, 15, 21], but integrated over the complement of $\mathcal{D}_n$. In terms of the mapping f, the conserved area $|\bar{\mathcal{D}}_i|$ can be written as

$$\begin{aligned} |\bar{\mathcal{D}}_i| &= \left| \int_0^{2\pi} d\alpha \left(\Re\left[f(e^{i\alpha},t)\right] - x(t)\right) \partial_\alpha \Im\left[f(e^{i\alpha},t)\right] \right| \\ &= \pi R^2(t) - \eta^2 \int_0^{2\pi} d\alpha\, \Re\left[\beta(e^{i\alpha},t)\right] \partial_\alpha \Im\left[\beta(e^{i\alpha},t)\right]. \end{aligned} \tag{3.3}$$

Now introducing the time independent length R_0 through $|\bar{\mathcal{D}}_i| = \pi R_0^2$, we find $R(t) = R_0 + \mathcal{O}(\eta^2)$, which proves that R is time independent within linear perturbation theory. In what follows we will use R_0 as our length scale, introducing

$$\epsilon = \frac{\ell}{R_0} \quad \text{and} \quad \tau = \frac{2}{1+\epsilon}\frac{t}{R_0}, \tag{3.4}$$

and rescaling f and Φ by factors $1/R_0$. We note that within a dimensionless time interval τ of order unity, the streamer moves a distance of the order of its size.

With the thus simplified ansatz (3.2), equations (2.7) and (2.8) evaluated to first order in η take the form

$$\begin{cases} \Re\left[\omega(\partial_\omega - \partial_\tau)\beta - \dfrac{1+\epsilon}{2}\omega\partial_\omega\chi\right] = 0, \\ \Re\left[\epsilon(\omega^2+1)\omega\partial_\omega\beta - (1+\epsilon)(1+\epsilon\omega\partial_\omega)\chi\right] = 0, \end{cases} \quad \text{for } \omega \in \partial\mathcal{U}_\omega. \tag{3.5}$$

Since β and χ are holomorphic for $\omega \in \mathcal{U}_\omega$, these equations imply

$$\begin{cases} \omega(\partial_\omega - \partial_\tau)\beta - \dfrac{1+\epsilon}{2}\omega\partial_\omega\chi = 0, \\ \epsilon(\omega^2+1)\omega\partial_\omega\beta - (1+\epsilon)(1+\epsilon\omega\partial_\omega)\chi = ia(t), \end{cases} \quad \text{for } \omega \in \mathcal{U}_\omega, \tag{3.6}$$

where $a(t)$ is some real function of time. χ is eliminated by substituting the expressions for $\partial_\omega\chi$ and $\partial_\omega^2\chi$ from the first equation and its derivative into the second equation differentiated with respect to ω. This yields

$$\mathcal{L}_\epsilon \beta = 0, \tag{3.7}$$

where $\mathcal{L}_\epsilon$ is the operator

$$\mathcal{L}_\epsilon = \frac{\epsilon}{2}\,\partial_\omega\,(\omega^2-1)\omega\,\partial_\omega + \epsilon\,\omega\partial_\omega\partial_\tau + (1+\epsilon)\,\partial_\tau - \partial_\omega. \tag{3.8}$$

3.3. Normal form of $\mathcal{L}_\epsilon$ and induced automorphisms of the unit disk. It is instructive to transform $\mathcal{L}_\epsilon$ to the normal form of a hyperbolic differential operator. We introduce

$$T = \tanh \frac{\tau}{2}, \tag{3.9}$$

mapping the time interval $\tau \in [0, \infty[$ to $T \in [0, 1[$, and

$$\zeta = \frac{\omega + T}{1 + \omega T}, \tag{3.10}$$

to find

$$\mathcal{L}_\epsilon = \epsilon h(\zeta, T)\partial_T \partial_\zeta + \frac{\partial h(\zeta, T)}{\partial T}\partial_\zeta + (1 + \epsilon)\partial_T, \tag{3.11}$$

$$h(\zeta, T) = \frac{\omega}{\partial_\zeta \omega} = \frac{(\zeta - T)(1 - T\zeta)}{1 - T^2}. \tag{3.12}$$

This identifies the manifolds $T = \text{const}$ or $\zeta = \text{const}$ as the characteristic manifolds of our problem for all $\epsilon \neq 0$.

As function of the "time-like" parameter T, $0 \leq T < 1$, the transformation $\zeta = \zeta(\omega, T)$ in (3.10) represents a semigroup of automorphisms of the unit disk, with fixed points

$$\zeta = \omega = \pm 1.$$

For $T \to 1$, corresponding to $\tau \to \infty$, all points $\omega \neq -1$ are mapped into $\zeta = +1$, so that the large time behavior of any perturbation is governed by this attractive fixed point.

3.4. Analytical solutions of (3.7) for special values of ϵ. The general solution of (3.7) can be found analytically for the special values $\epsilon = 0$, $\epsilon = \pm 1$, and $\epsilon = \infty$. In the unregularized case $\epsilon = 0$, evidently any function

$$\beta(\omega, \tau) = \tilde{\beta}(\omega + \tau)$$

is a solution, and any singularity of $\tilde{\beta}$ found in the strip

$$0 < \Re[\omega] < \infty, \quad -1 \leq \Im[\omega] \leq 1,$$

will lead to a breakdown of perturbation theory within finite time. This is the fingerprint of the ill-posedness of the problem for $\epsilon = 0$.

For $\epsilon = -1$, $\beta(\omega, \tau)$ generically for all $\tau > 0$ has a logarithmic singularity at $\omega = -T(\tau)$. We recall that negative values of $\epsilon = \ell/R_0$ imply negative thickness of the screening layer and thus are of no physical interest.

The case $\epsilon = +1$ is discussed in detail in the remainder of the paper. Though a regularization length ℓ identical to the object size R_0 is somewhat artificial, it is accessible to rigorous analytical treatment and, as explained in section 1.2, we expect it to reveal generic features of the behavior for all $\epsilon > 0$.

This is supported by the results for $\epsilon = \infty$ which show essentially the same features as the results for $\epsilon = 1$ below. Though the limit $\epsilon \to \infty$ is physically absurd when applied to streamers, it is worth studying with respect to the properties of the operator $\mathcal{L}_\epsilon$, and we present a short discussion in the appendix.

4. Strong screening: Analytical results for $\epsilon = 1$.

4.1. Analytical solution of the general initial value problem. With the form (3.11) of $\mathcal{L}_\epsilon$, the PDE (3.7) for $\epsilon = 1$ reduces to

$$\partial_T \left(2 + h(\zeta, T)\partial_\zeta\right) \beta = 0, \tag{4.1}$$

showing that the function

$$G(\zeta) = \left(2 + h(\zeta, T)\partial_\zeta\right) \beta \tag{4.2}$$

is independent of T. To determine β, we use (3.12), $h(\zeta, T) = \omega/\partial_\zeta \omega$, to find

$$\left(2 + \omega\partial_\omega\right) \beta(\omega, \tau) = G(\zeta), \quad \zeta = \zeta(\omega, T(\tau)). \tag{4.3}$$

The solution regular at $\omega = 0$ takes the form

$$\beta(\omega, \tau) = \int_0^\omega \frac{x\, dx}{\omega^2}\, G\left(\frac{x + T(\tau)}{1 + xT(\tau)}\right). \tag{4.4}$$

A second independent solution is singular in $\omega = 0$:

$$\beta_{\text{sing}}(\omega, \tau) \equiv \frac{1}{\omega^2}. \tag{4.5}$$

The function G in the regular solution (4.4) is determined by the initial condition $\beta(\omega, 0)$ through

$$G(\omega) = \left(2 + \omega\partial_\omega\right) \beta(\omega, 0). \tag{4.6}$$

It thus is holomorphic for ω in the unit disk $\mathcal{U}_\omega$, and all derivatives exist on $\partial\mathcal{U}_\omega$, since we assume the initial surface to be smooth. Equation (4.4) then shows that $\beta(\omega, \tau)$ inherits these properties for all $\tau < \infty$.

4.2. Automorphism of the unit disk and a bound on the perturbation. It is now clear that the automorphisms $\zeta(\omega, T)$ of $\mathcal{U}_\omega$ from (3.12) contain the basic dynamics, and, as shown in the appendix, this also holds for $\epsilon = \infty$. This is to be contrasted to the unregularized case $\epsilon = 0$, where the dynamics amounts to a translation of the unit disk. With the present dynamics, in the course of time larger and larger parts $\mathcal{U}(\delta)$ of the unit disk $\mathcal{U}_\omega$ are mapped to an arbitrarily small neighborhood $|\zeta - 1| < \delta$ of the attractive fixed point $\zeta = 1$. According to (4.4) and (4.6), the initial condition in the neighborhood $|\omega - 1| < \delta$ then determines the evolution of $\beta(\omega, \tau)$ in all $\mathcal{U}(\delta)$. As a consequence, any pronounced structure found initially near ω_0, $|\omega_0 - 1| > \delta$, is convected towards $\omega = -1$. Quantitatively this behavior is embodied in (4.17) below, and explicit examples will be presented in section 5; see, in particular, Figure 5.4(b).

For the further discussion we normalize $G(\omega)$ so that

$$\max_{|\omega|=1} |G(\omega)| = 1. \tag{4.7}$$

Equations (4.4), (4.7) yield a bound on $\beta(\omega, \tau)$:

$$|\beta(\omega, \tau)| \le \frac{1}{2}, \quad |\omega| \le 1, \quad 0 \le T \le 1. \tag{4.8}$$

Thus the perturbation can shift the position of the streamer by at most $\eta/2$, and therefore it cannot affect the asymptotic velocity of the propagation.

4.3. Center of mass motion for $0 \le \tau < \infty$. In precise terms the position of the streamer can be defined as the center of mass

$$z_{\rm cm} = x_{\rm cm} + iy_{\rm cm} = \frac{1}{|\bar{\mathcal{D}}_i|}\int_{\mathcal{D}_i} dx\, dy\, (x+iy), \tag{4.9}$$

where the integral is related to the first order Richardson moment. Evaluating (4.9) and (4.4), we find to first order in η

$$z_{\rm cm} = \tau + \eta\, \beta(0,\tau), \tag{4.10}$$

$$\beta(0,\tau) = \frac{G(T(\tau))}{2}. \tag{4.11}$$

Here τ is the uniform translation of the unperturbed circle. The additional center of mass motion (4.11) for all times is explicitly given by the initial condition $\beta(\omega,0)$ through (4.6) and the transformed time variable $T(\tau)$ from (3.9); for $\tau \to \infty$, it approaches $\beta(0,\tau) \to G(1)/2$.

4.4. Internal motion: Convergence along a universal slow manifold for $\tau \to \infty$. We now concentrate on the perturbation of the circular shape, given by

$$\tilde{\beta}(\omega,\tau) = \beta(\omega,\tau) - \beta(0,\tau). \tag{4.12}$$

The explicit expression

$$\tilde{\beta}(\omega,\tau) = \int_0^1 d\rho\, \rho \left[G\left(\frac{\rho\omega + T}{1+\rho\omega T}\right) - G(T)\right] \tag{4.13}$$

yields

$$\lim_{\tau\to\infty} \tilde{\beta}(\omega,\tau) = 0 \tag{4.14}$$

for arbitrary G, i.e., for arbitrary initial condition (4.6). Thus the shape perturbation converges to zero as $\tau \to \infty$, and the circular shape is linearly stable.

We note that this holds despite the fact that the limits $\omega \to -1$ and $\tau \to \infty$ (i.e., $T \to 1$) do not commute:

$$\lim_{T\to 1}\lim_{\omega\to -1} G(\zeta(\omega,T)) = G(-1),$$
$$\lim_{\omega\to -1}\lim_{T\to 1} G(\zeta(\omega,T)) = G(+1).$$

This peculiar behavior near the backside of the streamer, at $\omega = -1$, shows up only in the rate of convergence.

Investigating the rate of convergence for $\tau \to \infty$, we first exclude a neighborhood of $\omega = -1$ and expand G in the integral (4.13) as

$$G\left(\frac{\rho\omega + T}{1+\rho\omega T}\right) = G(T) + (1-T^2)\,\frac{\rho\omega}{1+\rho\omega T}\, G'(T) + \mathcal{O}(1-T^2)^2,$$
$$\text{where } G'(\omega) = \partial_\omega G(\omega).$$

With

$$1 - T^2 = 4e^{-\tau} + \mathcal{O}(e^{-2\tau}),$$

the integral yields

$$\frac{\tilde{\beta}(\omega,\tau)}{G'(1)} = \frac{4}{\omega^2}\left[\ln(1+\omega) - \omega + \frac{\omega^2}{2}\right] e^{-\tau} + \mathcal{O}(e^{-2\tau}), \tag{4.15}$$

valid for

$$|1+\omega| \gg |\omega| e^{-\tau}.$$

Thus outside the immediate neighborhood of $\omega = -1$, the shape for all smooth initial conditions with $G'(1) \neq 0$ converges exponentially in time as $e^{-\tau}$ along a universal path in function space, given in (4.15). For $G'(1) = 0$ the first nonvanishing term in the expansion of G dominates the convergence.

To analyze the neighborhood of $\omega = -1$ we take the limit $\tau \to \infty$, with

$$s = (1+\omega)e^{\tau} \tag{4.16}$$

fixed. We find

$$\begin{aligned}\frac{\tilde{\beta}(\omega,\tau)}{G'(1)} &= 4\left(\ln(2+s) - \tau\right) e^{-\tau} \\ &\quad + \left\{ 2G'(1) + 4\ln\left(\frac{2+s}{4}\right)\left(G'\left(\frac{s-2}{s+2}\right) - G'(1)\right)\right. \\ &\quad \left. + (2+s)\left(G(1) - G\left(\frac{s-2}{s+2}\right)\right) - 4\int_0^{4/(2+s)} dy \ln y\, G''(1-y)\right\} \frac{e^{-\tau}}{G'(1)} \\ &\quad + \mathcal{O}\left(\tau e^{-2\tau}\right).\end{aligned} \tag{4.17}$$

In terms of ω, the first contribution on the right-hand side takes the form

$$4\left(\ln(2+s) - \tau\right) e^{-\tau} = 4e^{-\tau} \ln\left(2e^{-\tau} + 1 + \omega\right),$$

which shows that a logarithmic cut of $\tilde{\beta}(\omega,\tau)$ reaches $\omega = -1$ for $\tau \to \infty$, but with a prefactor vanishing exponentially in that limit. We thus have found a weak anomaly of the asymptotic relaxation near $\omega = -1$: In a spatial neighborhood of order $e^{-\tau}$ the exponential relaxation is modified by a factor τ. Furthermore, as mentioned above, all the initial structure of $\beta(\omega, 0)$ is compressed into that region. This is obvious from the occurrence of $G\left(\frac{s-2}{s+2}\right)$ etc. in (4.17).

To summarize, we have found that the shape of the interface for $\tau \to \infty$ converges to the circle along a universal slow manifold (4.15), except for a weak anomaly (4.17) at the backside at $\omega = -1$.

4.5. (Non)analyticity of temporal eigenfunctions. In many cases, a full dynamical solution for arbitrary initial values cannot be found, and rather temporal eigenfunctions are searched for. However, in the present problem, functions $\beta(\omega,\tau)$ resulting from smooth initial conditions cannot exhibit exponential behavior in time for all τ, $0 \leq \tau < \infty$. This is seen easily by introducing

$$G(x) = \hat{G}\left(\frac{x-1}{x+1}\right), \tag{4.18}$$

writing $G(\zeta)$ in the equivialent form

$$G\left(\frac{\omega+T}{1+\omega T}\right) = \hat{G}\left(\frac{\omega-1}{\omega+1}\,e^{-\tau}\right), \tag{4.19}$$

and substituting this form into (4.4). Postulating strict exponential time behavior $\beta \sim e^{-\lambda\tau}$, one finds

$$\beta(\omega,\tau) \propto e^{\lambda\tau}\,\beta_\lambda(\omega), \quad \beta_\lambda(\omega) = \int_0^1 d\rho\,\rho\left(\frac{\omega\rho-1}{\omega\rho+1}\right)^\lambda. \tag{4.20}$$

Any eigenfunction $\beta_\lambda(\omega,0)$ with $\lambda \neq 0$ clearly is singular at $\omega=+1$, at $\omega=-1$, or at both points. It therefore conflicts with smooth initial conditions. On the other hand, omitting a neighborhood of $\omega=-1$, eigenfunctions exist for all $-\lambda \in \mathbf{N}_0$.

4.6. Completeness of the eigenfunctions near $\omega = 1$. In some neighborhood of $\omega=1$, we can even show that any regular solution $\beta(\omega,\tau)$ can be expanded in terms of the "eigenfunctions" $\beta_{-n}(\omega)$, $n \in \mathbf{N}_0$. This results from the Taylor expansion

$$\hat{G}(y) = \sum_{n=0}^{\infty} \hat{g}_n y^n, \tag{4.21}$$

which by assumption converges in a disk of radius $\hat{r} > 0$. Rewriting (4.4) as

$$\begin{aligned}\beta(\omega,\tau) &= \int_0^1 \frac{x\,dx}{\omega^2}\,G\left(\frac{x+T}{1+xT}\right) - \int_\omega^1 \frac{x\,dx}{\omega^2}\,G\left(\frac{x+T}{1+xT}\right)\\ &= \frac{M(T)}{\omega^2} - \sum_{n=0}^{\infty}\hat{g}_n\,e^{-n\tau}\int_\omega^1 \frac{x\,dx}{\omega^2}\left(\frac{1-x}{1+x}\right)^n\end{aligned} \tag{4.22}$$

and $\beta_{-n}(\omega)$ in a similar form as

$$\beta_{-n}(\omega) = \frac{M_n}{\omega^2} - \int_\omega^1 \frac{x\,dx}{\omega^2}\left(\frac{1-x}{1+x}\right)^n, \tag{4.23}$$

we find

$$\beta(\omega,\tau) = \frac{M(T)}{\omega^2} + \sum_{n=0}^{\infty}\hat{g}_n\left[\beta_{-n}(\omega) - \frac{M_n}{\omega^2}\right]e^{-n\tau}. \tag{4.24}$$

Provided that $e^{-\tau} < \hat{r}$, we can separate the sum into the contribution $\propto 1/\omega^2$ and the rest. Since both $\beta(\omega,\tau)$ and $\beta_{-n}(\omega)$ are regular at $\omega=0$, the contributions $\propto 1/\omega^2$ have to cancel, which yields the final result

$$\beta(\omega,\tau) = \sum_{n=0}^{\infty}\hat{g}_n\,\beta_{-n}(\omega)\,e^{-n\tau}. \tag{4.25}$$

This result is valid for $e^{-\tau} < \hat{r}$ in the disk

$$\left|\frac{1-\omega}{1+\omega}\right| e^{-\tau} < \hat{r}.$$

It generalizes the asymptotic result (4.15). Indeed, the universal shape relaxation found in (4.15) together with the center of mass relaxation (4.11) precisely follows the slowest eigenfunction from (4.21) with $\lambda = -n = -1$. Furthermore this result shows that the range of validity of the expansion (4.25) increases with τ and asymptotically covers the whole complex plane except for the special point $\omega=-1$.

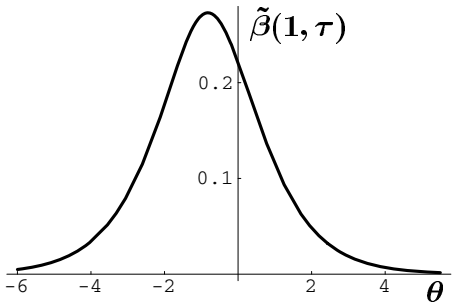

FIG. 4.1. $\tilde{\beta}(e^{i\alpha},\tau)$ *from* (4.27) *for* $\alpha = 0$ *as a function of subtracted time* $\theta = \tau - \ln 2k$.

4.7. Intermediate temporal growth and coupling of Fourier modes. Having found that the space of regular functions does not allow for strictly exponential time behavior, we now consider the typical time variation of smooth perturbations. Before the exponential relaxation sets in, such perturbations typically will grow, and this growth can be quite dramatic. As an illustration we consider a perturbation defined by

$$G(\omega) = \omega^k, \quad k \gg 1,$$

corresponding to initial conditions

$$\beta(\omega, 0) = \frac{\omega^k}{k+2}. \tag{4.26}$$

For $T = 1 - e^{-\theta}/k$, corresponding to times $\tau = \theta + \ln(2k) + \mathcal{O}(1/k)$, we can write

$$G\left(\frac{\omega+T}{1+\omega T}\right) = \left(\frac{1-\frac{e^{-\theta}}{1+\omega}\frac{1}{k}}{1-\frac{\omega e^{-\theta}}{1+\omega}\frac{1}{k}}\right)^k = \exp\left[-e^{-\theta}\frac{1-\omega}{1+\omega}\right]\left(1+\mathcal{O}\left(\frac{1}{k}\right)\right),$$

where we again exclude some neighborhood of $\omega = -1$. Substituting this expression into (4.13), we find on the unit circle $\omega = e^{i\alpha}$

$$\begin{aligned}&\tilde{\beta}(e^{i\alpha},\tau)\\ &\quad = \int_0^1 d\rho\,\rho \exp\left[-e^{-\theta}\frac{1-\rho^2-2i\rho\sin\alpha}{1+\rho^2+2\rho\cos\alpha}\right] - \frac{1}{2}\exp\left[-e^{-\theta}\right] + \mathcal{O}\left(\frac{1}{k}\right).\end{aligned} \tag{4.27}$$

Figure 4.1 shows this function, evaluated at $\alpha = 0$ ($\omega = 1$). The behavior is quite peculiar. Up to times of order $\ln k$ the perturbation stays of order $1/k \ll 1$, then it increases roughly exponentially up to values of order 1, and finally it decreases again exponentially, approaching the slow manifold (4.15). Thus for very large k the initial perturbation $\beta(\omega, 0) \sim 1/k$ in some time interval can be amplified by a factor of order k, and (4.27) shows that the leading behavior in that time interval is independent of k.

Closer analysis shows that in terms of a formal Fourier expansion

$$\tilde{\beta}(e^{i\alpha},\tau) = \sum_{n=1}^{\infty} a_n(\tau) e^{in\alpha}, \tag{4.28}$$

the amplification is carried by the low modes, $n = \mathcal{O}(1)$. As will be illustrated by an explicit example below (cf. Figure 5.2(b)), in such a mode representation the time evolution feeds the strength of the perturbation successively into lower and lower modes. This is equivalent to the observation that the automorphism $e^{i\alpha} \to \zeta(e^{i\alpha}, T)$ drives all the perturbative structure towards $\alpha = \pi$ and smooths the remainder of the interface. Note, however, that, starting with a perturbation $\sim \omega^k$, in the course of time modes $n > k$ are also (weakly) populated to build up a complicated structure near $\omega = -1$. We recall that for the unregularized model $\epsilon = 0$, the time evolution of a perturbation $\propto \omega^k$ populates only modes $k \le n$ [4].

4.8. Motion of the zeros of $\partial_\omega f$ and cusps. So far we have shown that the propagating circle is linearly stable; i.e., we implicitly considered perturbations of infinitesimal strength η. The full nonlinear evolution of a finite perturbation is beyond the scope of this paper. Still, it clearly is a question of practical interest, whether a finite perturbation evolving under the linearized dynamics for all times satisfies the assumptions underlying the conformal mapping approach. For the mapping to stay conformal, all the zeros of $\partial_\omega f(\omega, \tau)$ must stay outside the unit circle. Thus, here we analyze the roots of the equation

$$0 = \partial_\omega f(\omega, \tau) = -\frac{1}{\omega^2} + \eta\, \partial_\omega \beta(\omega, \tau). \tag{4.29}$$

Using (4.3), (4.4), we can rewrite this equation as

$$2\eta \int_0^1 d\rho\, \rho \left[G\left(\frac{\omega + T}{1 + \omega T}\right) - G\left(\frac{\rho\omega + T}{1 + \rho\omega T}\right)\right] = \frac{1}{\omega}. \tag{4.30}$$

With our normalization (4.7) of G, for all ω in the closed unit disk the left-hand side of this equation is bounded by $2|\eta|$. We conclude that the bound

$$|\eta| < \frac{1}{2} \tag{4.31}$$

guarantees that within the framework of first order perturbation theory the mapping stays conformal for all times. We now will show that in general this bound cannot be improved.

For $\tau \to \infty$, zeros of $\partial_\omega f(\omega, \tau)$ reach $\omega = -1$, which is a consequence of the fact that in this limit an infinitesimally small neighborhood of $\omega = -1$ under the mapping $\omega \to \zeta$ is mapped essentially on the whole complex plane. We now analyze this limit for the simple example $G(\omega) = \omega$. Substituting this form into the asymptotic behavior (4.17) and using the definition (4.16) of s, we find

$$\partial_\omega \beta = \frac{4}{2 + s} + \mathcal{O}(\tau e^{-\tau}).$$

Equation (4.29) reduces to $s = 4\eta - 2$, showing that a zero ω_0 of $\partial_\omega f(\omega, \tau)$ approaches $\omega = -1$ as

$$\omega_0 = -1 + (4\eta - 2)e^{-\tau}.$$

For ω_0 to come from outside the unit circle we clearly must have

$$\Re[\eta] < \frac{1}{2}. \tag{4.32}$$

To get some feeling for the estimate (4.31), we note that for $G(\omega) = \omega^k$ the map initially (for $\tau = 0$) is conformal provided that $|\eta| < 1 + 2/k$. We conclude that under the linearized dynamics a large part of smooth initial conditions relaxes to the circle.

Throughout this section we have assumed the initial boundary to be smooth, so that all derivatives $\partial_\omega^n G(\omega)$ exist on the boundary $|\omega| = 1$. Inspecting the results, it is obvious that this assumption can be considerably relaxed, since only those derivatives which show up explicitly have to exist. Thus, for exponential relaxation (4.15) outside the neighborhood of $\omega = -1$ to prevail, the existence of $\partial_\omega G(\omega)$ is sufficient, which amounts to the condition that the curvature of the initial boundary is well defined. For the circle to be linearly stable, as in (4.14), it is sufficient that $G(e^{i\alpha})$ is bounded and continuous, which implies that the boundary has a well-defined slope.

If the initial boundary shows a cusp, the time evolution sensitively depends on the details. If the cusp is found in the forward direction, so that $G(\omega)$ diverges for $\omega \to 1$, the streamer will be strongly accelerated. In a related model [12], such an effect has been pointed out before. Furthermore, the shape will not relax to a circle, and the conformal map will presumably break down at finite time. If the cusp does not affect the analyticity of $G(\omega)$ near $\omega = 1$, it is convected towards the back and broadened, whereas the front of the streamer approaches the circular shape. Still, however, conformality of the map may break down at finite time.

5. Explicit examples for $\epsilon = 1$. We here illustrate the general results by some examples.

5.1. The evolution of Fourier perturbations. We first consider perturbations of the form

$$\beta^{[k]}(\omega, 0) = \frac{\omega^k}{k+2}, \quad \text{i.e., } G(\omega) = \omega^k. \tag{5.1}$$

The integral (4.4) is easily evaluated to yield

$$\begin{aligned}\beta^{[k]}(\omega,\tau) = \frac{1}{2\omega^2 T^2}\Bigg\{ & T^k + \left((T\omega)^2 - 1\right)\zeta^k \\ & + k\left(1 - T^2\right)\Bigg[T^k - (\omega T + 1)\zeta^k + \frac{1 + k + T^2(1-k)}{T^k} \\ & \cdot \left(\ln(1+\omega T) - \sum_{\nu=1}^{k-1} \frac{T^\nu}{\nu}(\zeta^\nu - T^\nu)\right)\Bigg]\Bigg\},\end{aligned} \tag{5.2}$$

where $T = T(\tau)$ and $\zeta = \zeta(\omega, T(\tau))$ are given by (3.9) or (3.10), respectively. In Figure 5.1 we have plotted snapshots of the resulting motion of the interface, determined as

$$z = x + iy = \frac{1}{\omega} + \tau + \eta\,\beta^{[k]}(\omega,\tau), \quad \omega = e^{i\alpha}, \quad 0 \le \alpha \le 2\pi. \tag{5.3}$$

The direction of motion, i.e., the positive x-direction, is downwards. Together with the moving interface, we show the unperturbed circular streamer at different times as gray disks with the center moving according to

$$z_{\mathrm{cm}}(\tau) = \tau + \frac{\eta}{2}\,G(T(\tau)) = \tau + \frac{\eta}{2}\tanh^k\frac{\tau}{2}, \tag{5.4}$$

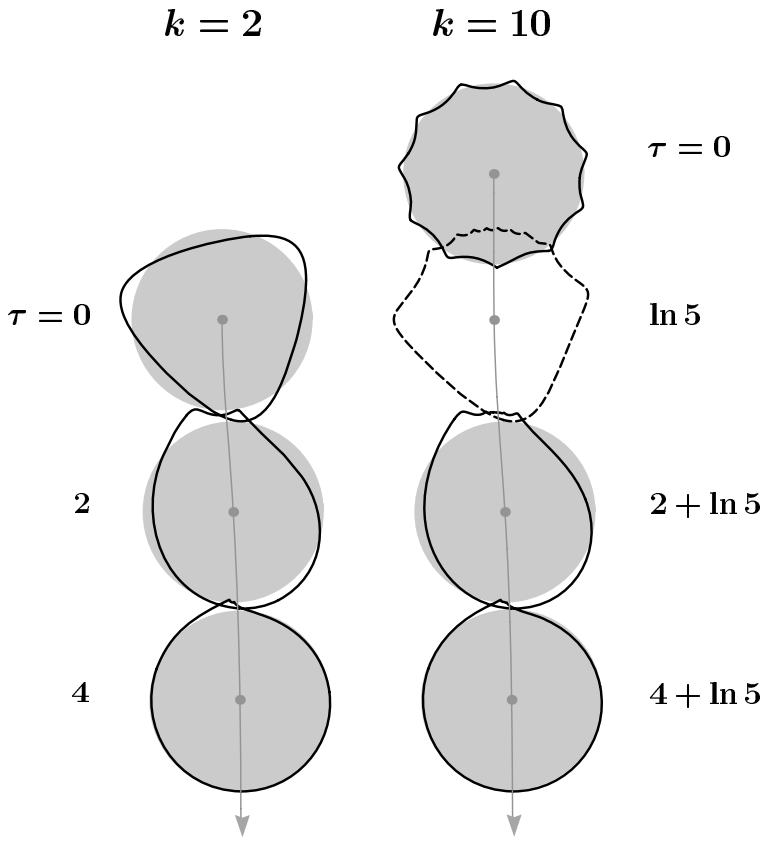

FIG. 5.1. *Snapshots of the evolution of the streamer for $k = 2$ (left column) and $k = 10$ (right column) at the indicated instants of time. The solid lines represent the perturbed interfaces. The gray disks move with the center of mass velocity* (5.4) *of the perturbed circles. One gray disk has been omitted for clarity. See the text for further discussion.*

as predicted for the center of mass motion for the perturbed streamer in (4.10).

In Figure 5.1 we perturbed the circle by $\eta\,\beta^{[k]}$, $k = 2$ or $k = 10$, using the same parameter $\eta = 0.6e^{i\pi/4}$ in both cases. The starting position for $k = 10$ is shifted relative to that for $k = 2$ by a distance corresponding to $\Delta\tau = \ln 5$. As discussed below (4.27), for $1 \ll k_1 < k_2$ we expect

$$\beta^{[k_1]}(\omega, \tau) \approx \beta^{[k_2]}(\omega, \tau + \ln(k_2/k_1)).$$

Figure 5.1 illustrates that such a "universality" for the gross structure holds down to very small k. (Of course the choice of differing values of η would distort the figures and mask this feature.) Basically during time evolution the initial maximum closest to the forward direction is smeared out and builds up the asymptotic circle, whereas all other structures are compressed at the backside. For $k = 10$ the complicated structure at the back is magnified in Figure 5.2(a). Figure 5.2(b) shows the time dependence of the coefficients a_n of the low modes $e^{in\alpha}$ in the expansion (4.28), again for $k = 10$. It illustrates how the strength of the perturbation cascades downwards in n and increases in time, until it is completely absorbed into the lowest mode, i.e., the overall shift of the circle. We should recall, however, that modes $n > k$ are also weakly populated to build up the structure at the back.

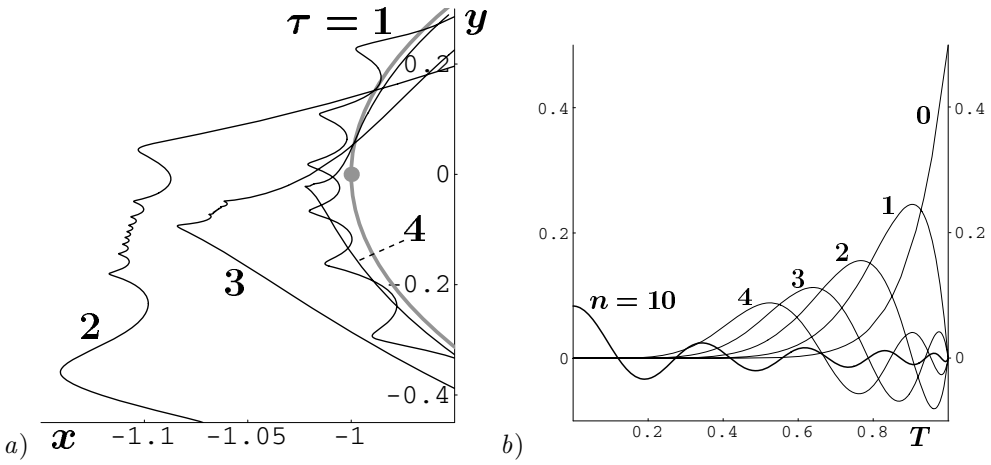

FIG. 5.2. (a) *Magnified plot of the backside of the streamer for* $k = 10$, $\eta = 0.6\, e^{i\pi/4}$ *(as in the right column of Figure* 5.1*) for the* τ *values given. The overall motion is subtracted. We observe the compression of the fine structure and the intermediate growth of the perturbation. Asymptotically for* $\tau \to \infty$, *the structure converges to the gray circle. In the comoving frame, the gray dot marks* $x + iy = -1$, *which is the point to which the structure finally is contracted. Note that the scale of* x *is stretched compared to that of* y, *and that the figure is turned relative to Figure* 5.1. (b) *The amplitudes* a_n *as in* (4.28) *as a function of* T *for* $k = 10$*; the values of* n *are given.*

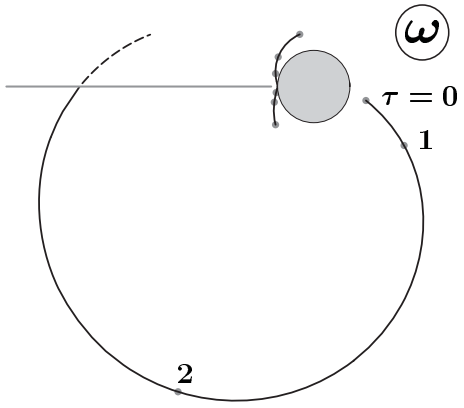

FIG. 5.3. *Motion of the zeros of* $\partial_\omega f$ *in the* ω*-plane for* $k = 2$ *and* $\eta = 0.6\, e^{i\pi/4}$ *(as in the left column of Figure* 5.1*). The dots give the position for* $\tau = 0, 1, 2$. *The horizontal line is the cut for* $\tau = 2.51$, *where one zero enters the second sheet (broken curve). The unit disk is also shown.*

For $k = 2$, Figure 5.3 shows the motion of the zeros of $\partial_\omega f(\omega, \tau)$ in the complex ω-plane, as discussed in section 4.8. It corresponds to the $k = 2$ part of Figure 5.1. Two zeros, which initially are close to the backside of the unit circle, approach $\omega = -1$ for $\tau \to \infty$. They clearly are associated with the two maxima that in the comoving frame are convected towards $z = x + iy = -1$. The third zero, originally found close to $\omega = +1$, after a large excursion leaves the physical sheet at time $\tau \simeq 2.51$. The logarithmic cut is on the negative axes, with the branchpoint $\omega_{\rm bp} = -1/T(\tau)$ reaching $\omega = -1$ for $\tau \to \infty$.

5.2. The evolution of localized perturbations. We finally consider some more localized perturbation, defined by

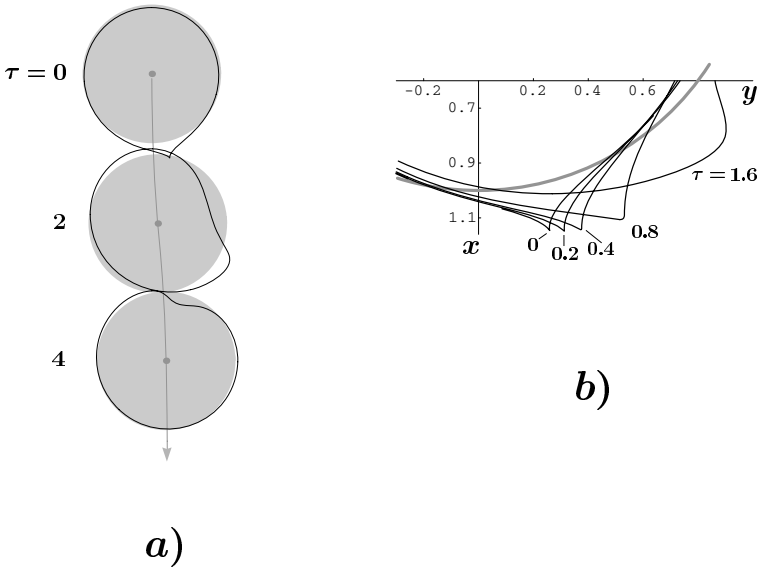

FIG. 5.4. (a) *Time evolution of a localized perturbation as described in the text.* (b) *Evolution of the initial peak for shorter times as indicated. The overall motion of the streamer is subtracted. A part of the asymptotic circle is shown in gray.*

$$G(\omega) = \frac{(1-\gamma)e^{i\alpha_0}}{\omega - \gamma e^{i\alpha_0}}, \quad \gamma > 1, \tag{5.5}$$

corresponding to an initial perturbation

$$\eta\,\beta(\omega,0) = \eta\,\frac{(1-\gamma)\gamma}{\omega^2}\,e^{2i\alpha_0}\left[\ln\left(1-\frac{\omega}{\gamma}\,e^{-i\alpha_0}\right) - \frac{\omega}{\gamma}\,e^{-i\alpha_0}\right]. \tag{5.6}$$

The result for $\beta(\omega,\tau)$ reads

$$\beta(\omega,\tau) = \frac{(\gamma-1)e^{i\alpha_0}}{\gamma e^{-i\alpha_0} - T(\tau)}\left\{\frac{T(\tau)}{2b(\tau)} - \left(1-\frac{T(\tau)}{b(\tau)}\right)\frac{\ln(1+b(\tau)\omega) - b(\tau)\omega}{(b(\tau)\omega)^2}\right\}, \tag{5.7}$$

where

$$b(\tau) = \frac{1 - T(\tau)\gamma e^{i\alpha_0}}{T(\tau) - \gamma e^{i\alpha_0}}. \tag{5.8}$$

We note that $b(\tau) \to 1$ for $T(\tau) \to 1$, so that in the large time limit the logarithmic cut reaches $\omega = -1$. As discussed in the context of (4.17), this is a generic feature of the present problem. Our choice of parameters ($\gamma = 1.1$, $\alpha_0 = -\pi/12$, $\eta = 1.5$) almost produces a cusp in the initial condition: The only zero of $\partial_\omega f(\omega,0)$ is found at $\omega_0 = 1.001\exp(-.243i)$. This zero, however, is driven away from the unit circle and leaves the physical sheet. Another zero, which entered the physical sheet somewhat earlier, for $\tau \to \infty$ reaches $\omega = -1$. Figure 5.4(a) shows snapshots of the time evolution of the perturbed interface in a representation like Figure 5.1. It illustrates how the peak is rapidly smeared out and the interface becomes smooth. Figure 5.4(b) follows the evolution of the peak for short times and shows how it is convected and broadened.

We finally note that, in the special case where the initial peak strictly points in the forward direction ($\alpha_0 = 0$), convection cannot take place. The peak simply is broadened and vanishes, whereas some new peak shows up at the back for intermediate times.

Appendix A. The limit $\epsilon \to \infty$. For $\epsilon \to \infty$, the PDE (3.7) with the form (3.11) of $\mathcal{L}_\epsilon$ reduces to

$$\Big(h(\zeta,T)\,\partial_\zeta + 1\Big)\,\partial_T\,\hat\beta(\zeta,T) = 0, \quad \text{where } \hat\beta(\zeta,T) \equiv \beta(\omega,\tau). \tag{A.1}$$

Equation (A.1) allows for a large set of solutions obeying the same initial condition

$$\beta(\omega,0) = \beta_0(\omega), \tag{A.2}$$

but imposing regularity on the unit disk $\mathcal{U}_\omega$, we single out the simple form

$$\beta(\omega,\tau) = \beta_0(\zeta). \tag{A.3}$$

Thus for $\epsilon = \infty$, the dynamics is simply given by the automorphisms $\omega \longrightarrow \zeta(\omega,T)$. This implies that $\beta(\omega,\tau)$ is bounded uniformly in τ as

$$\big|\beta(\omega,\tau)\big| \le \max_{\omega\in\partial\mathcal{U}_\omega} \big|\beta_0(\omega)\big|, \tag{A.4}$$

so that in contrast to the case $\epsilon = 1$, there is no intermediate growth of the perturbations.

The shift of the center of mass is given by (cf. (4.10))

$$\beta(0,\tau) = \beta_0(T(\tau)) = \beta_0(1) - 2\,\beta_0'(1)\,e^{-\tau} + \mathcal{O}\left(e^{-2\tau}\right), \tag{A.5}$$

and except for the point $\omega = -1$, the shape again converges exponentially in time to the circle along the universal slow manifold

$$\beta(\omega,\tau) - \beta(0,\tau) = \beta_0'(1)\,\frac{4\,\omega}{1+\omega}\,e^{-\tau} + \mathcal{O}\left(e^{-2\tau}\right); \tag{A.6}$$

cf. (4.15) for $\epsilon = 1$. Again the neighborhood of $\omega = 1$ for time $\tau = 0$, more precisely $\beta_0(1)$ and $\beta_0'(1)$, determines the long time convergence. Since by assumption $\beta_0(\omega)$ is analytical at $\omega = 1$, evidently an eigenfunction expansion in the sense of subsection 4.5 exists.

The only major difference compared to the case $\epsilon = 1$ concerns the point $\omega = -1$. Clearly,

$$\beta(-1,\tau) \equiv \beta_0(-1) \tag{A.7}$$

independently of τ, and indeed for $\tau \to \infty$ the conformality of the mapping breaks down in the neighborhood of $\omega = -1$ since $\partial_\omega\beta(\omega,\tau)\big|_{\omega=-1}$ diverges.

Acknowledgments. We acknowledge helpful and motivating discussions with F. Brau, A. Doelman, J. Hulshof, H. Levine, L. P. Kadanoff, S. Tanveer, and S. Thomae.

REFERENCES

[1] U. Ebert, W. van Saarloos, and C. Caroli, *Streamer propagation as a pattern formation problem: Planar fronts*, Phys. Rev. Lett., 77 (1996), pp. 4178–4181.
[2] M. Arrayás, U. Ebert, and W. Hundsdorfer, *Spontaneous branching of anode-directed streamers between planar electrodes*, Phys. Rev. Lett., 88 (2002), 174502.
[3] M. Arrayás and U. Ebert, *Stability of negative ionization fronts: Regularization by electric screening?*, Phys. Rev. E (3), 69 (2004), 036214.
[4] B. Meulenbroek, A. Rocco, and U. Ebert, *Streamer branching rationalized by conformal mapping techniques*, Phys. Rev. E (3), 69 (2004), 067402.
[5] U. Ebert, C. Montijn, T. M. P. Briels, W. Hundsdorfer, B. Meulenbroek, A. Rocco, and E. M. van Veldhuizen, *The multiscale nature of streamers*, Plasma Sources Sci. Technol., 15 (2006), pp. S118–S129.
[6] D. Bensimon, L. P. Kadanoff, S. Liang, B. I. Shraiman, and C. Tang, *Viscous flows in two dimensions*, Rev. Modern Phys., 58 (1986), pp. 977–999.
[7] L. I. Rubinstein, *The Stefan Problem*, Transl. Math. Monogr. 27, AMS, Providence, RI, 1971.
[8] P. S. Ho, *Motion of inclusion induced by a direct current and a temperature gradient*, J. Appl. Phys., 41 (1970), pp. 64–68.
[9] M. Mahadevan and R. M. Bradley, *Stability of a circular void in a passivated, current-carrying metal film*, J. Appl. Phys., 79 (1996), pp. 6840–6847.
[10] G. Taylor and P. G. Saffman, *A note on the motion of bubbles in a Hele-Shaw cell and porous medium*, Quart. J. Mech. Appl. Math., 12 (1959), pp. 265–279.
[11] S. Tanveer and P. G. Saffman, *Stability of bubbles in a Hele-Shaw cell*, Phys. Fluids, 30 (1987), pp. 2624–2635.
[12] D. C. Hong and F. Family, *Bubbles in the Hele-Shaw cell: Pattern selection and tip perturbations*, Phys. Rev. A (3), 38 (1988), pp. 5253–5259.
[13] V. M. Entov, P. I. Etingof, and D. Ya. Kleinbock, *Hele-Shaw flows with a free boundary produced by multipoles*, European J. Appl. Math., 4 (1993), pp. 97–120.
[14] B. Meulenbroek, U. Ebert, and L. Schäfer, *Regularization of moving boundaries in a Laplacian field by a mixed Dirichlet-Neumann boundary condition: Exact results*, Phys. Rev. Lett., 95 (2005), 195004.
[15] S. D. Howison, *Complex variable methods in Hele-Shaw moving boundary problems*, European J. Appl. Math., 3 (1992), pp. 209–224.
[16] F. Brau, A. Luque, B. Meulenbroek, U. Ebert, and L. Schäfer, *Construction and test of a moving boundary model for negative streamer discharges*, Phys. Rev. E (3), submitted; available online from http://arxiv.org/abs/0707.1402.
[17] Yu. E. Hohlov and M. Reissig, *On classical solvability for the Hele-Shaw moving boundary problems with kinetic undercooling regularization*, European J. Appl. Math., 6 (1995), pp. 421–439.
[18] M. Reissig, S. V. Rogosin, and F. Hübner, *Analytical and numerical treatment of a complex model for Hele-Shaw moving boundary value problems with kinetic undercooling regularization*, European J. Appl. Math., 10 (1999), pp. 561–579.
[19] S. J. Chapman and J. R. King, *The selection of Saffman-Taylor fingers by kinetic undercooling*, J. Engrg. Math., 46 (2003), pp. 1–32.
[20] S. Tanveer, F. Brau, U. Ebert, and L. Schäfer, in preparation.
[21] S. Richardson, *Hele Shaw flows with a free boundary produced by the injection of fluid into a narrow channel*, J. Fluid Mech., 56 (1972), pp. 609–618.